

Impact of an Active Sgr A* on the Synthesis of Water and Organic Molecules Throughout the Milky Way

Chang Liu,¹ Xian Chen,^{1,2} and Fujun Du³

¹*Department of Astronomy, School of Physics, Peking University, Beijing 100871, China*

²*Kavli Institute for Astronomy and Astrophysics, Beijing 100871, China*

³*Purple Mountain Observatory, Chinese Academy of Sciences, Nanjing 210008, China*

Abstract

Sgr A*, the supermassive black hole (SMBH) in our Galaxy, is dormant today, but it should have gone through multiple gas-accretion episodes in the past billions of years to grow to its current mass of $4 \times 10^6 M_\odot$. Each episode temporarily ignites the SMBH and turns the Galactic Center into an active galactic nucleus (AGN). Recently, we showed that the AGN could produce large amount of hard X-rays that can penetrate the dense interstellar medium in the Galactic plane. Here we further study the impact of the X-rays on the molecular chemistry in our Galaxy. We use a chemical reaction network to simulate the evolution of several molecular species including H_2O , CH_3OH , and H_2CO , both in the gas phase and on the surface of dust grains. We find that the X-ray irradiation could significantly enhance the abundances of these species. The effect is the most significant in those young, high-density molecular clouds, and could be prominent at a Galactic distance of 8 kpc or smaller. The imprint in the chemical abundance is visible even several million years after the AGN turns off.

Keywords: astrochemistry — Galaxy: abundances — ISM: abundances — ISM: molecules — X-rays: ISM

1. Introduction

Supermassive black holes (SMBHs) are ubiquitous in the centers of massive galaxies (Kormendy & Ho 2013). In theory, a SMBH grows to its current mass mainly through multiple episodes of gas accretion (Volonteri 2010). In each accretion phase a significant fraction of the gravitational energy of the gas is released in the form of radiation, and the galaxy center consequently becomes an active galactic nucleus (AGN, Soltan 1982). Analysis of the luminosity function of bright AGNs indicates that the accretion episodes may add up to about (1 – 10)% of the lifetime of a galaxy (Hopkins & Hernquist 2009; Shankar et al. 2009). The SMBHs in the mass range of $(10^6 - 10^7) M_\odot$ on average are more active in the sense that they become AGNs every $10^7 - 10^8$ years while each active phase only lasts $10^5 - 10^6$ years (Hopkins et al. 2006).

The center of the Milky Way (MW) also harbors a SMBH. It coincides with the bright radio source Sagittarius A* (Sgr A*) and the mass is estimated

to be $4 \times 10^6 M_\odot$ (Genzel et al. 2010). This black hole (BH) is dormant today, but in the past it should have been active according to the close relationship between SMBH growth and AGN activity (Mezger et al. 1996). One interesting discovery in the last decade is that Sgr A* may be an AGN just several million years (Myrs) ago. This picture is supported by a series of findings, including the Fermi bubble (Su et al. 2010), the bright emission of $H\alpha$ lines in the Magellanic Stream (Bland-Hawthorn et al. 2013), and the young stellar disk around Sgr A* which is reminiscent of a relic accretion disk (see Chen & Amaro-Seoane 2015, for a review). The peak luminosity of that recent AGN is unclear and the current estimations fall in a broad range of (3 – 100)% of the Eddington limit $L_{\text{Edd}} \simeq 5 \times 10^{44} \text{ erg s}^{-1}$ (Nayakshin & Cuadra 2005; Bland-Hawthorn et al. 2013). Such a high level of activity is not completely unexpected given the aforementioned frequent activity of low-mass BHs.

Not many works have explored the impact of an active Sgr A* on the habitability of the MW. Early studies identified X-ray and cosmic rays as a potential threat to lives but they lacked a theoretical framework to quantify the damage (Clarke 1981; Lavolette 1987; Gonzalez

2005). Amaro-Seoane & Chen (2019, Paper I) adopted an empirical AGN spectral energy distribution (SED) and calculated the extinction of light in the Galactic plane. They found that hard X-rays (> 2 keV) could reach Earth unattenuated and the corresponding flux is comparable to an X-class solar flare. They also suspected that the high X-ray irradiation may have a noticeable impact on the molecular chemistry in the MW. Other works neglected the attenuation of light and focused on the evaporation of planet atmosphere during the AGN irradiation (Balbi & Tombesi 2017; Chen et al. 2018; Forbes & Loeb 2018; Wislocka et al. 2019). Their general conclusion is that mass loss is significant only within a distance of 1 kpc from Sgr A*. More recently, Lingam et al. (2019) explored possible beneficial effects associated with the AGN irradiation, such as a prebiotic synthesis of the building blocks of biomolecule and a powering of photosynthesis on free-floating planets. Based on the estimation of the UV flux, they reached a similar conclusion that only in the central kpc of the MW are these effects important.

In this work, we continue our early study of the impact of an active Sgr A* on the habitability of the MW. We focus on hard X-ray irradiation because, unlike optical and UV, hard X-ray photons are not attenuated by the gas in the Galactic plane and hence could reach large distances (see Paper I). It is known, from studying the molecular clouds in star-forming regions, that hard X-rays could enhance the abundance of organic molecules such as CN, C₂H, HCN by 2 – 6 orders of magnitude (Krolik & Kallman 1983; Lepp & Dalgarno 1996). The main reason is that X-rays, by ionizing atoms and molecules, create energetic electrons (Shull & van Steenberg 1985; Maloney et al. 1996), which, by further interacting with the atoms and molecules, produce reactive ions and radicals (Herbst & Klemperer 1973; Herbst & van Dishoeck 2009a). Ions and radicals, compared to neutral species, react more quickly to produce complex molecules (Herbst & van Dishoeck 2009a; Wakelam et al. 2010).

Because of the close relationship between X-ray irradiation and the synthesis of organic molecules, we expect an imprint of the recent active Sgr A* in the abundance of complex molecules in the MW. This is a reasonable expectation also because abnormal molecular abundances have been detected in external galaxies with AGNs (Usero et al. 2004). For example, the column densities of H₂O and some organic species such as HCN, HCO⁺, and CH₃OH are particularly high in AGNs (González-Alfonso et al. 2010; Davies et al. 2012; Imanishi & Nakanishi 2014; Takano et al. 2014; Harada et al. 2018) compared to

those in MW clouds (see below). The canonical explanation of this enhancement is that the AGN produces an X-ray dominated region (XDR) within a distance of $10 - 10^2$ pc (Meijerink & Spaans 2005; Meijerink et al. 2007; Viti et al. 2014; Izumi et al. 2015). At such a close distance, the X-ray flux could be as high as $10^2 \text{ erg cm}^{-2} \text{ s}^{-1}$, which exceeds the UV radiation produced by the starburst in a galactic nucleus (typically $10 \text{ erg cm}^{-2} \text{ s}^{-1}$, e.g., García-Burillo et al. 2010; Izumi et al. 2015). As a result, the molecular clouds in this region are ionized mainly by X-rays and heated to a temperature of 100 – 200 K. Under these conditions, the synthesis of H₂O and organic molecules can be enhanced. Besides X-ray irradiation, mechanical heating due wind or jet also plays an important role in the enhancement of organic molecules, such as HCN (García-Burillo et al. 2014; Izumi et al. 2015; Martín et al. 2015).

Although these previous studies revealed a positive correlation between X-ray irradiation and the abundances of water and organic molecules, we cannot draw directly the conclusion that the past activities of Sgr A* have had a positive impact on the production of water and organic molecules in the MW. The reasons are as follows. (i) We are interested in the molecular clouds throughout the MW, with the distance from the Galactic Center ranging from hundreds of parsecs to ten kpc. In this distance range, the X-ray flux impinging on the clouds is not as strong as those shown above in AGNs. For example, in Paper I we showed that at the location of the solar system, which is 8 kpc from the Galactic Center, the X-ray flux during the active phase of Sgr A* is a few times $10^{-3} \text{ erg cm}^{-2} \text{ s}^{-1}$. Such a flux is not much higher than the UV-background radiation in the Galactic plane Draine (1978). Therefore, our molecular clouds are not in the XDR. In fact, neither the UV background nor the cosmic rays can be neglected in the chemistry model of these clouds. (ii) When the X-ray flux is as low as $0.1 \text{ erg cm}^{-2} \text{ s}^{-1}$, the molecular clouds would not be significantly heated by the X-ray ionization and could remain cold (< 50 K) (Meijerink et al. 2007). In such a “cold cloud”, the dominant chemical reactions and the reaction rates differ from those in an XDR (Herbst & van Dishoeck 2009a). It is worth noting that cold clouds represent the initial conditions for the formation of low-mass stars, such as our Sun, and may determine the early chemical composition of solar-like systems. Therefore, it is important to understand the potential impact of the X-ray irradiation on the synthesis of water and organic molecules in them.

In cold clouds, several molecules are synthesized at a relatively early stage, some of which are the

building blocks of more complex, larger molecules. Among these “zeroth-generation” species, water (H_2O), methanol (CH_3OH), and formaldehyde (H_2CO) are commonly found in the molecular clouds of the MW (Herbst & van Dishoeck 2009a). Therefore, they are particularly interesting to our study. (i) Water is an important molecule involved in the processes leading to the origin of life. It can be synthesized in gas as well as on the surface of dust grains. In cold clouds, the water vapor abundance (relative to H_2) is normally $10^{-10} - 10^{-8}$ (Snell et al. 2000), while the surface abundance of water ice is much higher, about 10^{-4} of H_2 (Bergin & Tafalla 2007). Around AGNs, the abundance of water vapor can be as high as 10^{-6} (González-Alfonso et al. 2010), confirming the positive effect of X-ray irradiation on the synthesis of water molecules. (ii) Methanol (CH_3OH) is one of the most common organic molecules detected in cold clouds (Herbst & van Dishoeck 2009b). Its abundance varies from 10^{-9} and below in the gas phase (10 K) to as high as $10^{-6} - 10^{-5}$ in ice (Herbst & van Dishoeck 2009b). In AGNs, the gas abundance is typically 10^{-7} (García-Burillo et al. 2010; Nakajima et al. 2015; Harada et al. 2018). These CH_3OH in XDRs may be produced on grains and then released into the gas due to shock. (iii) Formaldehyde (H_2CO) is often detected at the surface of a cold cloud. This species may be produced by grain processes deep in the cores of the cloud and later brought to the cloud surface by turbulence (Federman & Allen 1991). In cold clouds, the typical gas abundance is $10^{-10} - 10^{-9}$ (Carey et al. 1998), but in XDRs the abundance can be 1–2 orders of magnitude higher (Harada et al. 2015, 2018).

The chemical process which lead to the formation of large, organic molecules in the MW is still under intensive investigation, and the role of the X-rays from Sgr A* is unclear. As a first step towards understanding their possible relationship, we study in this work the synthesis of water and the “zeroth-generation” organic molecules in cold clouds. We pay particular attention to CH_3OH and H_2CO , for the reasons given above, but we also study several other organic molecules, such as HCN , HCO^+ , which are known to be enhanced in XDRs (Kohno et al. 2003; Usero et al. 2004; Davies et al. 2012; Imanishi & Nakanishi 2014; Viti et al. 2014; Martín et al. 2015).

This paper is organized as follows. In §2 we calculate the X-ray irradiation spectra at different distances from Sgr A*, and we also specify our X-ray chemical model, especially the processes associated with H_2O , CH_3OH , and H_2CO . In §3 we describe our simulation of the molecular chemistry induced by X-ray irradiation. The

results are presented in §4, where we show the dependence of the abundance of different molecules on the distance, column density, and lifetime of a molecular cloud. A possible diagnostics is provided in §5 for future observational test of our theoretical results. We discuss the caveats of our current model in §6 and finally summarize our conclusions in §7.

2. X-ray Chemistry in Molecular Clouds

2.1. X-ray Source

To calculate the X-ray flux during the AGN phase of Sgr A*, we use a numerical model which is described in detail in Liu et al. (2016). This model computes the SED of an accretion disk based on three parameters, the Eddington ratio defined as $\eta := L/L_{\text{Edd}}$ where L is the bolometric luminosity of the disk, the X-ray spectral index α , and the magnetic parameter β which characterizes the relative importance between the sum of the gas and radiative pressure and the magnetic pressure. In this model, hard X-rays are produced by a hot corona screening the disk. The solid curves in Figure 1 show the output SED as a function of the Eddington ratio. In the calculation we assume that $\alpha = 0.1$, $\beta = 100$, and the BH mass is $4 \times 10^6 M_{\odot}$. We find that when $\eta \gtrsim 1$, the X-ray flux above 2 keV is more or less constant, at a level of a few times $10^{-3} \text{ erg s}^{-1} \text{ cm}^{-2}$. This result from numerical simulation is consistent with our analytical estimation in Paper I. When $\eta \lesssim 0.5$, we find that the luminosity of hard X-ray falls linearly with decreasing Eddington ratio.

Soft photons are subject to extinction as they propagate in the Galactic plane. To quantify it, we adopt the empirical density profile of the atomic hydrogen $\rho_{\text{H}}(R)$ and molecular hydrogen $\rho_{\text{H}_2}(R)$ in the MW (McMillan 2017), and we use the software *Xspec*¹ to calculate the extinction. Since most molecular clouds are inside the Galactic plane, we only consider the horizontal (in-plane) gas distribution. The corresponding column density at a Galactic distance of R is

$$\Sigma(R) = \int_0^R [\rho_{\text{H}}(x) + \rho_{\text{H}_2}(x)] dx. \quad (1)$$

The residual SEDs at $R = 8 \text{ kpc}$, for example, are shown in Figure 1 as the dot-dashed curves. We can see that the optical and UV radiation is completely absorbed. For this reason, in our chemistry model we focus on the effects induced by X-rays.

2.2. X-ray Ionization

¹ <https://heasarc.gsfc.nasa.gov/xanadu/xspec/>

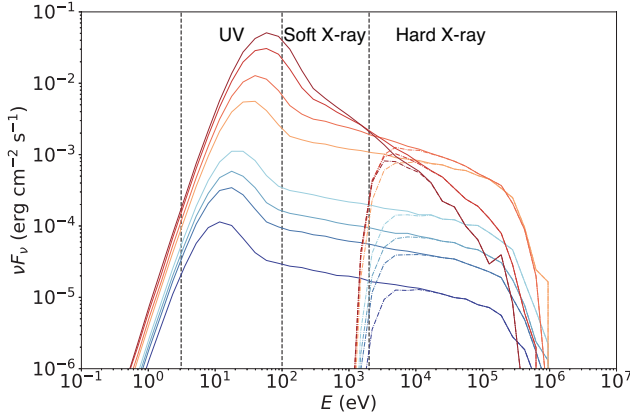


Figure 1. The SED of Sgr A* at a Galactic distance of 8 kpc. The solid curves show the unabsorbed SEDs of the AGN assuming a bolometric luminosity of (3.0, 2.0, 1.0, 0.5, 0.1, 0.05, 0.03, 0.01) times the Eddington luminosity. The dot-dashed ones account for the extinction at a Galactic distance of 8 kpc.

It is mainly through ionization that X-ray irradiation could affect the chemistry inside a molecular cloud (Maloney et al. 1996). Other effects, such as Coulomb heating, are less important in an environment where the ionization fraction x_e is relatively low. In our model we consider two types of ionization.

Primary ionization, also known as the direct photoionization, is caused by an X-ray photon striking an atom (e.g. Latif et al. 2015). The primary ionization rate for a given species i can be calculated with

$$\zeta_p^i = \int_{E_{min}}^{E_{max}} \frac{F(E)}{E} e^{-\tau(E)} \sigma^i(E) dE, \quad (2)$$

where $F(E)$ is the monochromatic X-ray flux incident on the surface of a molecular cloud, $\sigma^i(E)$ is the photoionization cross section given a photon energy of E (Verner et al. 1996), τ is the optical depth defined as

$$\tau(E) = \sum_{i=H,He} N_i \sigma^i(E), \quad (3)$$

and N_i is the column density of a species. In calculating the optical depth, we have taken into account the fact that H (mostly in molecular hydrogen) and He contribute to most of the opacity.

The photoelectrons released in primary ionization could further collide with other atoms and cause secondary ionization (Maloney et al. 1996; Stäuber et al. 2005). In principle, the secondary ionization rate can be calculated with

$$\zeta_{sec}^i = \int_{E_{min}}^{E_{max}} \frac{F(E)}{E} e^{-\tau(E)} N_{sec}(E, x_e) \sigma^i(E) dE, \quad (4)$$

where $N_{sec}(E, x_e)$ is the number of secondary ionization events produced by each photoelectron in average. If the energy of the photoelectron is E , this number can be calculated with

$$N_{sec}(E, x_e) = \frac{\eta_{ion}(x_e)E - E_{th}}{W(E)}, \quad (5)$$

where η_{ion} is the fraction of the photoelectron's energy which goes into secondary ionization, E_{th} is the ionization threshold of an atom, and W is the mean energy needed to produce an ion-electron pair. In practice, we simplify the calculation by adopting the ionization rates presented in Shull & van Steenberg (1985). These rates are derived from a Monte Carlo simulation of the secondary ionization of H and He atoms over a wide range of electron fraction ($0.0001 < x_e < 1$) and photoelectron energy (from 100 eV to several keV).

Although we have two types of ionization in our model, the secondary ionization rate predominates. For example, if we consider a typical value of $x_e \leq 1\%$ for a cold ($T \sim 10$ K) molecular cloud, approximately 40% of the energy of primary photoelectrons goes into secondary ionization. Since the ground state of neutral H has a ionization threshold $E_{th} = 13.6$ eV, using $\eta_{ion} = 40\%$ and $W(E) = E_{th}$, we find that for a typical primary photoelectron with $E = 1$ keV, the number for secondary ionization events it will cause is $N_{sec}(E, x_e) \approx 30$.

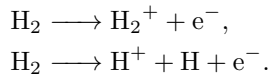
For H_2 , H and He, we consider both primary and secondary ionization. For heavy elements (C, N, O, etc.) and molecules (CO, CO_2 , etc.), we consider only the secondary ionization for simplicity. We assume that the ionizing electrons are mainly from the three most abundant neutral species, i.e., H_2 , H and He. Then the ionization rate of heavy elements and molecules can be derived from

$$\zeta^m = \frac{\sigma_{ei,m}(E)}{\sigma_{ei,H}(E)} \zeta_{sec}^H, \quad (6)$$

where $\sigma_{ei}(E)$ is the electron-impact cross section at energy E (Maloney et al. 1996; Ádámkóvics et al. 2011). We note that heavy elements are usually bound in molecules, but the current derivation of $\sigma_{ei}(E)$ assumes that the cross section is unaffected by the molecular binding energy. Moreover, we notice that the ratio of the cross sections, which appears in the last equation, is insensitive to E (Maloney et al. 1996). For this reason, we use the cross sections at $E = 50$ eV, which is the typical energy of the secondary electrons.

For completeness, we also consider the destruction of H_2 and several other molecules caused by photoionization. For example, photoionization of H_2 can have two possible outcomes, pure ionization and dissociation,

which can be expressed as



We take the branching ratio suggested by Krolík & Kallman (1983), that the fraction of pure ionization is approximately 80% and that for dissociation is 20%. For other atomic and molecular reactants, we adopt the same products from the OSU chemical database `osu_01_2007`², as well as the corresponding branching ratios for cosmic-ray ionization and dissociation. We choose this database because it was used by Wakelam & Herbst (2008) to explain the molecular abundances observed in the cold dense cores in the MW. These cores represent the initial conditions of the molecular clouds of our own interest. To be able to reproduce the results in Wakelam & Herbst (2008), we did not choose the latest chemical database provided by the OSU group. The later updates included more anions, which are more important for the formation of long carbon chains (Herbst & van Dishoeck 2009a).

2.3. Grain Processes

The surface of a dust particle (grain) is an important place for the synthesis of complex molecules. A grain accretes from the surrounding gas many molecular species to its surface, where these molecules can interact more frequently and the chemical reactions such as hydrogenation can proceed more efficiently. Since we are interested in the synthesis of H_2O , CH_3OH , and H_2CO (see §1), we include in our model the surface reactions containing the species made of H, C, N, O. Only those species with no more than two C atoms are selected since we do not study long-carbon-chain species in this work. Table 1 in Appendix A shows the relevant reactions, which are selected from the network presented in Hasegawa et al. (1992). The last column shows the activation energies for those reactions with high energy barriers. This network is sufficient to simulate the species we are interested in. The reaction parameters in this network are still frequently used today, although there are works which extend the reaction mechanisms so that the desorption energy may depend on the fraction of surface coverage by molecules (Garrod & Pauly 2011) and that the molecules in ice mantle could react with each other (Chang & Herbst 2014). More recent grain-surface chemical networks (e.g., Garrod et al. 2008) are usually concerned with the formation of more complex organic molecules, which is not the focus of the current

work. On one hand, the abundances of those very complex molecules are usually low, so that including them in our network should have a negligible effect on the species studied in this paper. On the other, it may be interesting to ask to what extent those more complex molecules are affected by the mechanisms discussed in the current paper, which may be a topic for future investigation.

We calculate the accretion rate of molecules onto dust grains following the method developed in Hasegawa et al. (1992). We consider accretion, via weak van der Waals forces (physisorption), onto “classic” dust grains, which have a fixed radius $r_d = 1000 \text{ \AA}$, a density of $\rho = 3 \text{ g/cm}^3$, and $N_s = 10^6$ sites for adsorption (the number of molecules that can be absorbed to and held on a dust grain). The dust temperature T_d is assumed to be the same as the gas temperature $T \sim 10 \text{ K}$, following the assumption in Hasegawa et al. (1992). This is a reasonable approximation for the clouds at $\gtrsim 2 \text{ kpc}$ but may be too crude for those at 1 kpc . This is because within 1 kpc from the AGN, the X-ray flux significantly exceeds $0.1 \text{ erg s}^{-1} \text{ cm}^{-1}$ so that heating due to ionization cannot be neglected given our cloud density of 10^4 cm^{-3} (Meijerink et al. 2007). Moreover, we did not consider the difference between the gas and dust temperatures because the difference is small due to the efficient gas-dust coupling at a high density of 10^4 cm^{-3} (Goldsmith 2001). Moreover, the reaction rates are insensitive to small temperature changes (at least in the range of temperature of our interest). For the gas-to-dust ratio in mass, we adopt the standard value of 100. We assume that the velocities of the gas species obey Maxwell distribution. For any species that strikes a dust grain, a sticking probability of 1 is assumed.

For the desorption of molecules, we consider three channels, namely, thermal desorption, cosmic-ray desorption, and photo-desorption. (i) Given the adsorption energy E_D and dust temperature T_d , the thermal evaporation rate can be calculated with $R_{\text{evap}} \propto E_D^{1/2} \exp[-E_D/kT_d]$ (Hasegawa et al. 1992), where k is the Boltzmann constant. The value of E_D for each species is from Allen & Robinson (1977) and Hasegawa & Herbst (1993). We note that although thermal evaporation is common, the rate is negligible for any species heavier than He because of the low temperature in our molecular clouds. (ii) The cosmic-ray induced desorption rates are calculated as in (Hasegawa & Herbst 1993). Every time a cosmic-ray particle strikes a dust grain, the dust temperature is assumed to rise to 70 K immediately and then drop via thermal desorption. (iii) Photo-desorption can be induced by either UV or X-ray photons. For UV-induced desorption, we assume a rate of 10^{-3} molecule per grain

² <https://faculty.virginia.edu/.archived/ericherb/research.html>

per incident UV photon for any species in our grain-surface network (also see Visser et al. 2011). Since UV-induced desorption depends strongly on the visual extinction, which is a function of the optical depths of a molecular cloud, we will study in §4.3 the dependence of the rate on the column density of the molecular cloud. The X-ray desorption processes are more complex (see Jiménez-Escobar et al. 2018 for a brief review) and not as well understood both in theory and in experiment. However, X-ray photons are more penetrative than UV photons, so that the interaction happens deeper inside the bulk of a grain and hence does not as often lead to desorption. Therefore, the X-ray desorption is less significant compared to UV photo-desorption and we neglect it in our model.

3. Simulation

We solve the evolution of the chemical network using the public package KROME³ (Grassi et al. 2014). The initial conditions are as follows. Our molecular cloud has a gas temperature of $T = 10$ K and a density of $n_{\text{H}} = 2 \times 10^4 \text{ cm}^{-3}$. The initial abundances of elements are taken from the EA2 model in Wakelam & Herbst (2008), which is based on the high-metal environment observed in the diffuse cloud of ζ Ophiuchi and is modified based on recent observations of cold cores. For the species at different depths of a molecular cloud, we assume that they follow the same initial abundances.

In our model, even when there is no X-ray irradiation, we include a low level of ionization caused by cosmic rays. The corresponding ionization rate is $\zeta = 1.3 \times 10^{-7} \text{ s}^{-1}$ per hydrogen atom (Wakelam & Herbst 2008). We also include a generic UV background according to Draine (1978). Given the UV flux, we calculate the photo-ionization and photo-desorption rates following the scheme presented in §2.

To simulate the impact of the AGN, we turn on X-ray chemistry in the network according to the method described in §2.2 and §2.3. The X-ray SED is calculated assuming a fiducial Eddington ratio of $\eta = 1$. The extinction of optical, UV, and soft-X-ray photons by the Galactic plane is taken into account following §2.1. Since hard X-rays have relatively low extinction in the Galactic plane, the flux decreases with the distance approximately as R^{-2} . The corresponding values are $(660, 120, 20, 4.2) \times 10^{-3} \text{ erg cm}^{-2} \text{ s}^{-1}$ at $R = (1, 2, 4, 8) \text{ kpc}$. The duration of the X-ray irradiation is set to 10^6 years, to be consistent with the empirical evidence (§1). After that, we turn off the X-ray and let

the network evolve for another 10^7 years. By the end of the simulation, we investigate the abundance of the molecular species at different Galactic distances to look for possible imprints of an AGN. In our fiducial model we use $R = 4 \text{ kpc}$ (§4.1). We also run simulations using $R = (1, 2, 8) \text{ kpc}$ for comparison (§4.2).

We notice that as the system evolves, the chemical abundance is no longer uniformly distributed inside a molecular cloud because the extinction of UV and X-ray radiation varies at different depth of the cloud. The depth h can be characterized by the column density of hydrogen, N_{H} , which is related to h as $N_{\text{H}} = n_{\text{H}} h$. Therefore, to understand the abundance of molecular species at different depth in a cloud, we run simulations using different N_{H} . Given the value of N_{H} , the extinction of X-ray inside the cloud is calculated using optical depth defined in Equation (3). For the extinction of UV photons, we use the empirical relationship

$$\frac{A_V}{N_{\text{H}}} = 5.3 \times 10^{-22} \text{ mag cm}^2 \quad (7)$$

which is caused mainly by dust (Draine 2011). For reference, the typical visual extinction A_V is 8 mag in a dense molecular cloud and could increase to 15 mag in dense cores (Tielens 2010). In our fiducial model, we set $N_{\text{H}} = 10^{22.5} \text{ cm}^{-2}$ and the corresponding A_V is 16.8. We also experiment with $N_{\text{H}} = 10^{22}$ and 10^{23} cm^{-2} for comparison and the results are shown in §4.3.

We also note that in our fiducial model the initial chemical abundance is out of equilibrium, in the sense that without X-ray irradiation the abundance would still evolve relatively quickly, on a timescale of $10^6 - 10^7$ years. Nevertheless, we choose this initial condition because it agrees better with the observed abundance in several molecular clouds (e.g. Wakelam & Herbst 2008; Quan & Herbst 2007). For old molecular clouds ($\sim 10^7$ years), the chemical abundance could significantly deviate from our initial condition. To account for this possibility, we run additional simulations in which we evolve our network for 10^7 years before we turn on the X-ray irradiation. The results are presented in §4.4.

4. Results

4.1. Fiducial Model

In our fiducial model, the Eddington ratio of the AGN is $\eta = 1$. The molecular cloud is at a Galactic distance of 4 kpc and has a column density of $N_{\text{H}} = 10^{22.5} \text{ cm}^{-2}$ ($A_V = 16.8$). The results for the chemical evolution are shown in Figures 2 and 3. In general, the abundances of molecules on the dust grain surface are several orders of magnitude higher than their gas-phase counterparts. This is mainly because at low temperatures (~ 10 K)

³ <http://kromepackage.org/>

molecules stay on the surface of dust grains, and the grain surface acts as a reaction container and a catalyst leading to much more efficient formation of H_2O , CH_3OH , etc.

For H_2O (Fig. 2), on the grain surface (lower panels), even without X-rays (the black dot-dashed curves) the abundance keeps growing during the first $10^5 - 10^6$ years and afterwards saturates. The increase is caused mainly by two surface reactions, (i) $\text{H}_2 + \text{OH} \longrightarrow \text{H}_2\text{O} + \text{H}$ and (ii) $\text{H} + \text{OH} \longrightarrow \text{H}_2\text{O}$. The first reaction usually predominates because of the high abundance of H_2 , even though the activation energy is high (Hasegawa et al. 1992). The second one has a much lower energy barrier but the rate is limited by the low concentration of atomic H at the grain surface. The saturation of the water surface abundance in the late stage is due to a balance between the photo-evaporation and the formation processes.

If we start X-ray irradiation at the very beginning (green solid curves), the H_2O surface abundance increases faster and in the end slightly exceeds that in the case without X-ray. We find that the first reaction is not significantly affected by the X-ray irradiation, because the H_2 surface abundance only slightly decreases. On the contrary, the second reaction becomes faster because the atomic hydrogen abundance increases significantly due to the X-ray dissociation of H_2 . After we remove the X-ray irradiation at the end of 10^6 years (green dashed curve), the surface abundance of H_2O stays more or less constant. The value is slightly lower than that in the case of X-ray irradiation because atomic H quickly recombine to form H_2 , thus the rate of the second reaction drops.

For the gas phase (the upper panels of Fig. 2), when there is no X-ray, the abundance of H_2O first increases until a plateau is reached around the time of $10^4 - 10^5$ years. During this period, ionization leads to the formation of H_3^+ , which is a highly reactive species that can quickly produce OH^+ , H_2O^+ , and H_3O^+ (Krolik & Kallman 1983). Gaseous water is synthesized mainly by the recombination of H_3O^+ with electrons. Around the time of 10^6 years, the abundance of gas H_2O starts to decrease because the materials such as OH^+ , H_2O^+ , and H_3O^+ run out following the exhaustion of O, so that the formation of H_2O slows down. The final gaseous abundance is limited mainly by the interaction with atomic cations, such as Si^+ through the ion-neutral reaction $\text{Si}^+ + \text{H}_2\text{O} \longrightarrow \text{HSiO}^+ + \text{H}$.

When X-ray irradiation is turned on, the behavior of the water abundance in the gas phase is similar to that on the grain surface. However, both the rise and fall of the H_2O abundance are more prominent, which leads to

a higher plateau around 3×10^5 yr and a lower abundance at about $\gtrsim 10^6$ yr. The sharper evolution is caused by the higher cation density during the X-ray ionization, such as H_3^+ , OH^+ , H_2O^+ , during the early formation stage of H_2O , as well as the higher abundance of Si^+ during the later stage of H_2O destruction. After we remove the X-rays, the abundance of H_2O first decreases but within about 10^5 years recovers the value which is seen in the case of no X-ray irradiation. The recovery is caused by the dissociative recombination, $\text{H}_3\text{O}^+ + \text{e}^- \longrightarrow \text{H}_2\text{O} + \text{H}$, as well as the photo-evaporation from the grain surface.

For CH_3OH , the evolution of the abundance after the first 10^6 yr is shown in the two upper panels of Figure 3. We do not show the evolution in the first 10^6 years because it is a monotonic increase. Also, we are more interested in the molecular abundances millions of years after the AGN turns off. At the grain surface (right panel), when there is no X-ray irradiation, the abundance is almost constant over 10^7 years of evolution. The dominant synthesis process is hydrogenation, via $\text{CO} \longrightarrow \text{HOC} \longrightarrow \text{CHOH} \longrightarrow \text{CH}_2\text{OH} \longrightarrow \text{CH}_3\text{OH}$. When X-ray irradiation is turned on, the abundance of CH_3OH becomes more than two orders of magnitude higher. The increase is caused by a faster hydrogenation process, as the result of a larger atomic-hydrogen abundance due to the X-ray disassociation. Even after we remove the X-ray, the CH_3OH surface abundance stays nearly the same. This is because in our model there is no chemical reaction at the grain surface for CH_3OH destruction (also see Hasegawa et al. 1992) and also the photo-evaporation of CH_3OH is inefficient.

In the gas phase (upper-left panel), without X-ray irradiation, the abundance of CH_3OH stays constant for about 10^6 years and afterwards slightly declines. Gaseous CH_3OH mainly comes from the grain surface, and the later decline is caused by the reactions with cations, e.g., $\text{CH}_3\text{OH} + \text{He}^+ \longrightarrow \text{OH}^+ + \text{CH}_3 + \text{He}$ / $\text{OH} + \text{CH}_3^+ + \text{He}$. With X-rays and for the particular Galactic distance of our choice, i.e., 4 kpc, the abundance of CH_3OH increases by about one order of magnitude relative to that in the case without X-rays. The increase is closely related to the enhancement of the CH_3OH abundance on dust grains. After we remove the X-rays, the abundance increases even more because cations recombine and the destruction of CH_3OH slows down.

For H_2CO , the results are shown in the lower two panels of Figure 3. Unlike CH_3OH which forms only at the grain surface, H_2CO can form both on the surface of grains, mainly through hydrogenation $\text{CO} \longrightarrow \text{HCO} \longrightarrow \text{H}_2\text{CO}$, and in gas phase, via $\text{CH}_3 + \text{O} \longrightarrow$

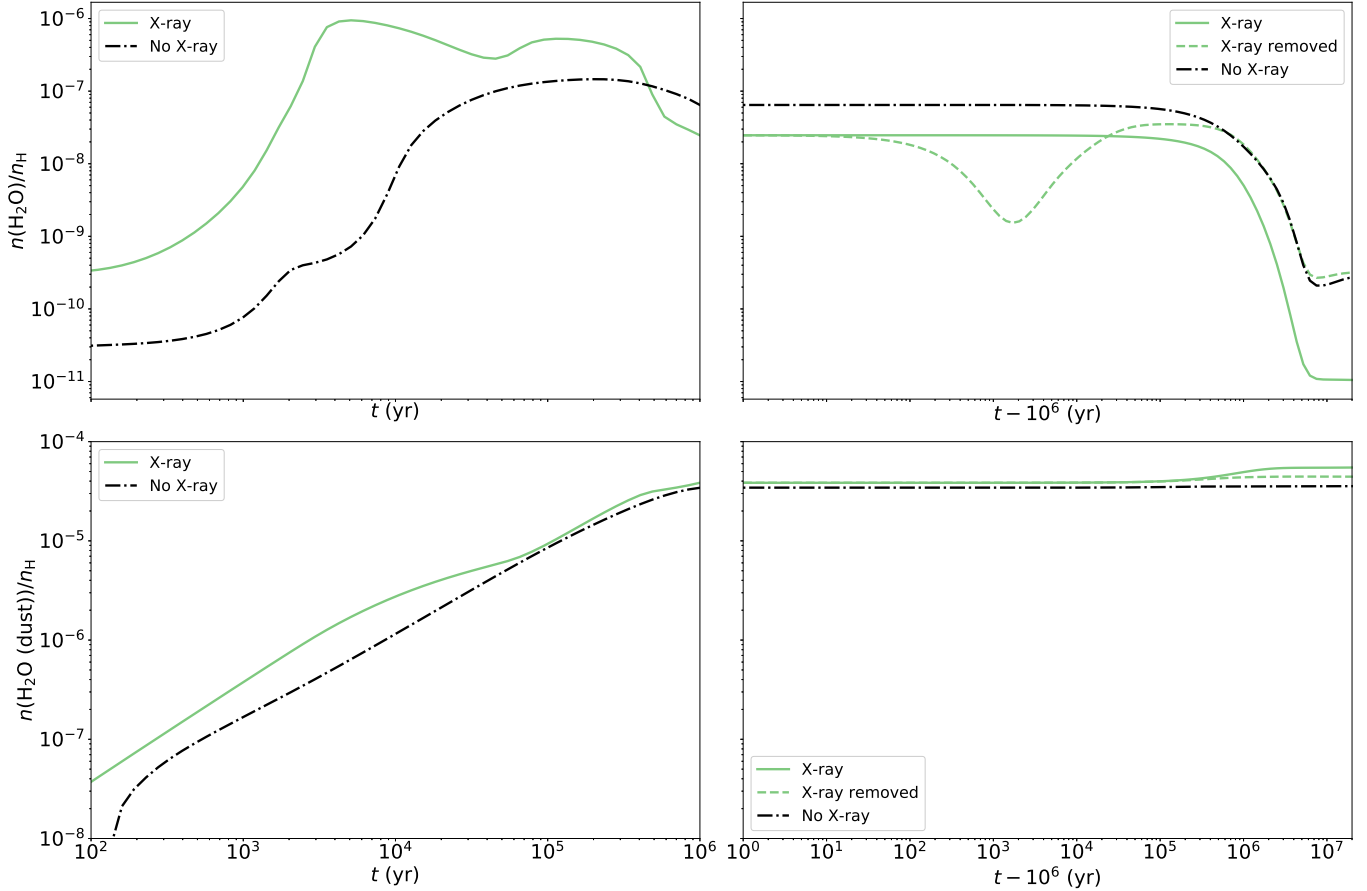


Figure 2. Abundances of H_2O in a molecular cloud 4 kpc away from the galactic center and with a hydrogen column density of $N_{\text{H}} = 10^{22.5} \text{ cm}^{-2}$. The upper panels show the abundance of H_2O in the gas phase and the lower ones show that at the grain surface. The left panels show the first 10^6 years of the chemical evolution and the right ones show the later 10^7 years. The green solid curves correspond to the model in which the AGN persists, while the green dashed ones correspond to the situation where the AGN is turned off after 10^6 years. For comparison, the results when there is no AGN irradiation is shown as the black dot-dashed curves.

$\text{H}_2\text{CO} + \text{H}$. Moreover, There is also one pathway for H_2CO on the grain surface to dissociate, $\text{H}_2\text{CO} + \text{H} \longrightarrow \text{HCO} + \text{H}_2$. The O atom can then be transferred to species like CO_2 through reaction $\text{O} + \text{HCO} \longrightarrow \text{CO}_2 + \text{H}$. Although the activation energy of this dissociation is high, the reaction rate is still orders of magnitude higher than photo-evaporation.

With these differences in mind, we can understand the behavior of H_2CO at the grain surface (lower-right panel). During the X-ray irradiation, the formation rate is first enhanced due to a higher hydrogenation rate. In the last several million years of our simulation the abundance of H_2CO significantly decreases, because the disassociation process becomes important and O atoms are slowly transferred to species like CO_2 . After we remove the X-ray irradiation, the decrease of the surface abundance of H_2CO becomes slower because the surface abundance of H falls substantially. Because the formation (hydrogenation) of H_2CO is also proportional to

the surface abundance of H, we do not see an increase of H_2CO after we remove the X-ray irradiation.

In the gas (lower-left panel), even without X-rays, the abundance of H_2CO drops by almost four orders of magnitude by the end of the 10^6 – 10^7 years of evolution. The drop is mainly caused by the exhaustion of CH_3 and O, so that the rate of the reaction $\text{CH}_3 + \text{O} \longrightarrow \text{H}_2\text{CO} + \text{H}$ significantly decrease by the end of our simulation. With X-rays, the abundance decreases relative to that in the case without X-ray irradiation, by a factor of a few. The drop is due to the higher abundance of cations. In this case, the destructive reactions, such as $\text{H}_2\text{CO} + \text{S}^+ \longrightarrow \text{HCO}^+ + \text{HS}$, become more efficient. When we remove the X-rays, the H_2CO abundance first recovers the value in the case of no X-ray irradiation and in about 10^6 years significantly decreases due to the exhaustion of CH_3 . Finally, the abundance balances at a value which is higher than that in the no-X-ray case, because more

CH₃ has been produced during the episode of X-ray irradiation.

For completeness, we show in the [Appendix B](#) the evolution of the other species that are often detected in molecular clouds. In general, we also find that their abundances with and without X-rays are different.

4.2. Distribution in the Galactic Disk

Since the X-ray flux decreases with increasing distance from the Galactic Center, we also explore the chemical evolution at different Galactic distances. The results are shown in Figure 4, where the column density of each cloud is still set to $N_{\text{H}} = 10^{22.5} \text{ cm}^{-2}$.

On the grain surface (right panels), when there is X-ray irradiation (solid curves), the abundance of H₂O keeps increasing as the Galactic distance decreases. The increase is caused by the higher abundance of atomic hydrogen as the ionization flux intensifies. For CH₃OH and H₂CO, however, the surface abundance maximizes at a Galactic distance of 4 – 8 kpc, and further increasing or decreasing the distance would both lead to a lower abundance. The location where these two abundances peak is determined by two competing processes. On one hand, an important precursor of both species, CO, can be destroyed by X-rays and hence cannot exist too close to the Galactic Center when the AGN is on. On the other, the abundance of H increases towards the AGN due to X-ray disassociation. These two processes balance at about 4 – 8 kpc and produce the highest abundance of CH₃OH and H₂CO there.

To understand the behavior of H₂O, CH₃OH, and H₂CO after we turn off the X-ray irradiation (dashed lines), we should first understand the evolution of H₂ and CO. The major difference between the two species is that while the H₂ abundance is lowered by several percents during the X-ray irradiation, the abundance of CO could be lowered by orders of magnitude depending on the Galactic distance. Therefore, after we turn off the X-rays, the abundance of H₂ only slightly increases in percentage, due to recombination, and recovers the equilibrium in the case of no X-rays, but the abundance of CO increases more drastically. The difference in the recovery rate causes the different behavior of H₂O versus CH₃OH and H₂CO at the grain surface. We can see that after we turn off X-rays, the surface abundance of H₂O increases slightly, because there is slightly more H₂ for the reaction $\text{H}_2 + \text{OH} \rightarrow \text{H}_2\text{O} + \text{H}$. For CH₃OH and H₂CO, however, there is a lot more CO produced within a short period of time, especially at small Galactic distances. For example, at 1 kpc the abundances of CH₃OH and H₂CO rise by orders of magnitude after the X-ray irradiation is turned off. One interesting result,

which is shared by all the three molecular species (H₂O, CH₃OH, and H₂CO) and at all the simulated Galactic distances, is that the final surface abundance after we remove X-rays is higher than the abundance in the case without X-ray irradiation.

In the gas phase (left panels), the behavior of H₂O, CH₃OH, and H₂CO also depends on the Galactic distance. For H₂O, the X-ray irradiation in general suppresses the abundance within a timescale of 10^7 years, because, as we have explained in §4.1, destructive cations form in large amount but water formation on the grain surface is relatively inefficient. Moreover, the final abundance decreases with decreasing distance, because the X-ray flux is higher at smaller distance. For CH₃OH and H₂CO, destructive cations also form due to the X-ray irradiation. That is why at small Galactic distances such as 1 and 2 kpc, the abundances of CH₃OH and H₂CO are suppressed when the AGN is on. However, at large distances such as 4 and 8 kpc, the abundances are not significantly suppressed and could even exceed those in the cases without X-rays. The reason is that at these distances the X-ray flux is not as strong so that CH₃OH and H₂CO form very fast on the grain surface, which, through photo-evaporation, could also enrich the gas.

After we turn off the X-ray irradiation, the gaseous abundances of H₂O, CH₃OH, and H₂CO all increase within a timescale of 10^7 years, regardless of the Galactic distance. The cause is mainly the recombination of cations, which in turn lowers the destruction rate. Photo-evaporation also contributes considerably. Even for H₂O, whose gaseous concentration is not as sensitive to the surface abundance, photo-evaporation enriches the gas species significantly after $\sim 5 \times 10^6$ years, when the dissociative recombination has significantly slowed down. We find that at all distances, after we remove the X-rays, the final abundances of gaseous H₂O, CH₃OH, and H₂CO exceed those in the case without an AGN or with a constant AGN.

These results suggest that a relatively short episode (10^6 years) of X-ray irradiation could indeed, in the following 10^7 years, leave an imprint in the molecular abundances throughout the MW.

4.3. Distribution Inside Molecular Cloud

To understand the distribution of H₂O, CH₃OH, and H₂CO as a function of the depth inside a molecular cloud, we compute the chemical evolution assuming different column densities (N_{H}) for the cloud. The results are shown in Figure 5. In these calculations, the Galactic distance of the cloud is fixed at 4 kpc.

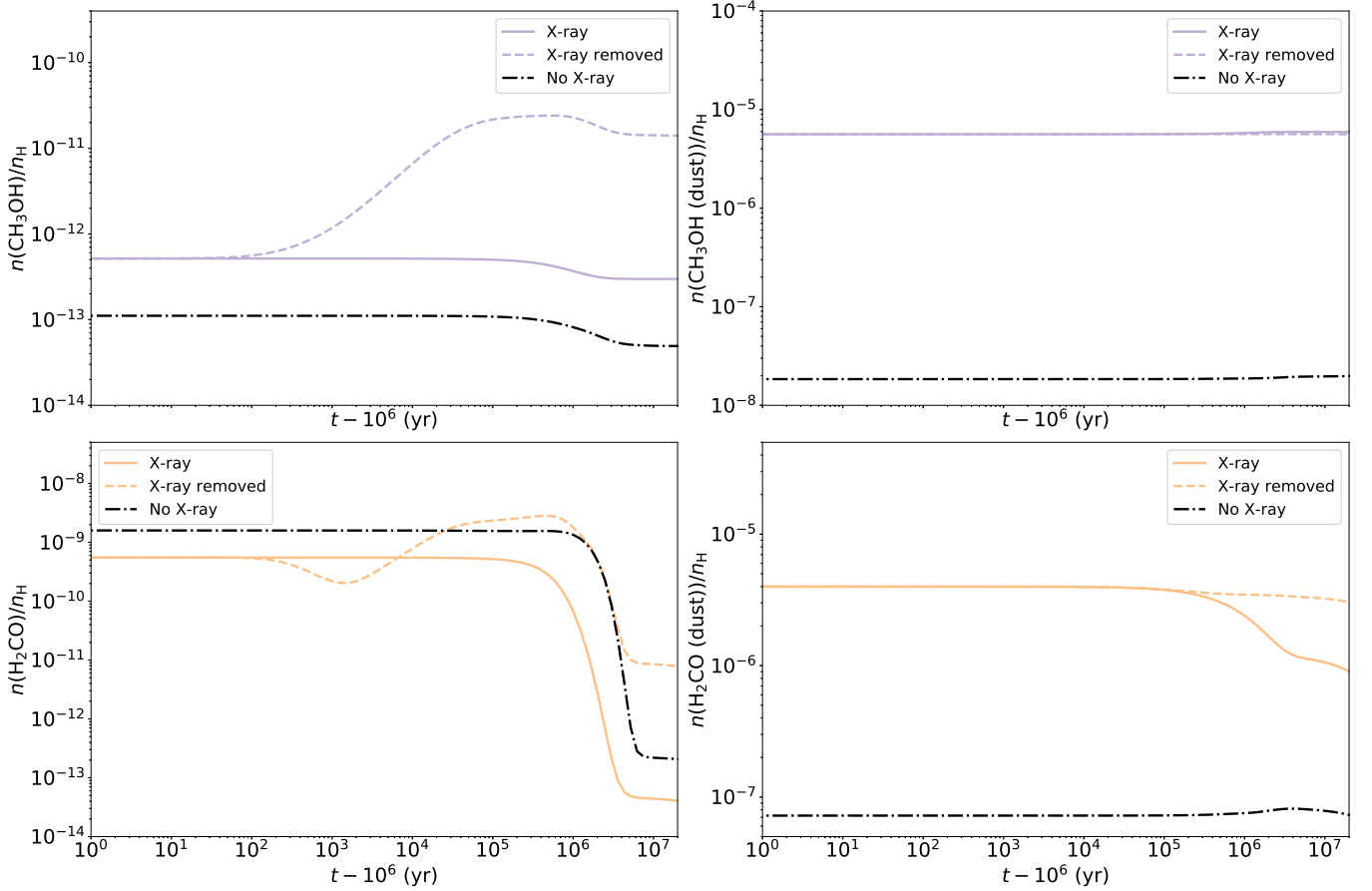


Figure 3. Evolution of the abundances of CH_3OH (upper) and H_2CO (lower) in the gas phase (left) and on the grain surface (right). The line styles have the same meanings as in Fig. 2.

We find that when the column density is high, i.e., $N_{\text{H}} = 10^{23} \text{ cm}^{-2}$ (or equivalently $A_V = 53$), the abundances (see the blue curves) are slightly, but systematically lower than those in the fiducial model. This trend can be seen both in the gas phase and on the grain surface. The main cause of this systematic change is the lower UV flux due to higher extinction. The hard X-ray flux from the AGN is only slightly attenuated inside the molecular cloud, and hence when we turn on and off the AGN the evolution of the three species is similar to the evolution in our fiducial model.

In low-extinction regions ($N_{\text{H}} = 10^{22} \text{ cm}^{-2}$, $A_V = 5.3$, the red curves), the surface abundances (right panels) are more significantly affected by the rise of the UV irradiation. Even when there is no X-ray radiation (dotted curves), the H_2O abundance is lower than that in the fiducial case by one order of magnitude. On the contrary, the surface abundances of H_2CO and CH_3OH are higher than those in the fiducial model. This result is caused by two competing processes. On one hand, surface species evaporate more rapidly in the presence of a higher UV flux. On the other, the higher density of H

due to UV ionization/dissociation enhances the rate of hydrogenation. Since the synthesis of H_2O uses mainly H_2 , not H, a higher UV flux would increase the evaporation rate more than the hydrogenation one, causing the surface abundance of water to decrease. For CH_3OH and H_2CO , the hydrogenation rate is relatively higher than the evaporation rate, so that the surface abundances increase when the UV flux becomes higher.

If we turn on X-rays, the surface abundances of all the three species increase (compare the red-dotted and the red-solid curves), because of an enhancement of the H density on the grain surface. However, compared to those in the high-extinction regions (blue solid curves), the surface abundances in the low-extinction regions is reduced, because of a higher evaporation rate induced by X-rays in the latter case. After we remove the X-ray irradiation, within $\sim 10^6$ years the abundances recover the values in the case of no X-rays. The quick recovery is closely correlated with the high reaction and evaporation rate in the low-extinction regions.

In the gas phase of the low-extinction regions (red curves in the left panels), the abundances of H_2O ,

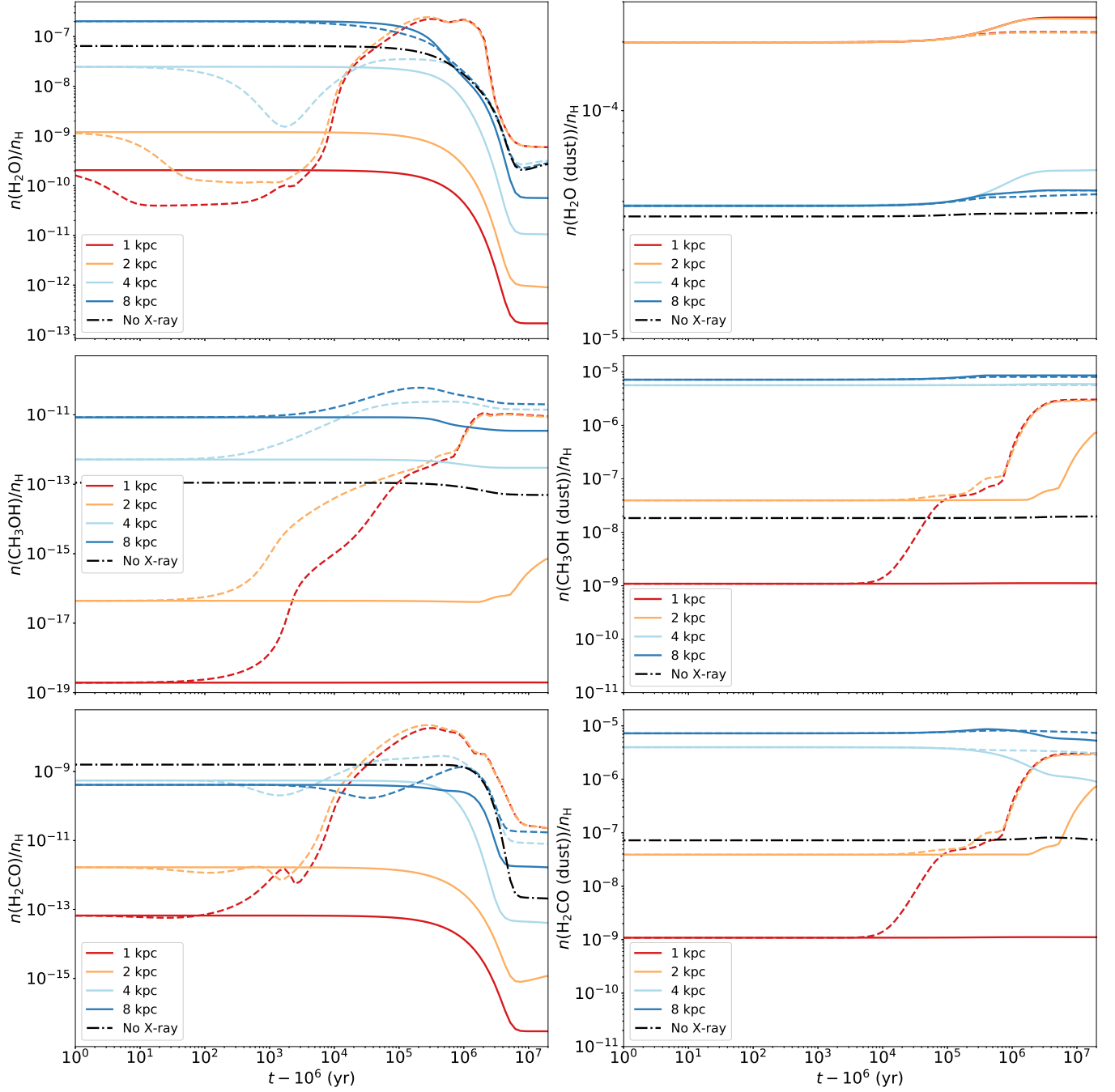


Figure 4. Evolution of the abundances of H_2O , CH_3OH , and H_2CO (from top to bottom) inside the molecular clouds at different Galactic distances (1, 2, 4, and 8 kpc). The left panels show the abundances in the gas phase and the right ones show the surface abundances. The lines styles have the same meanings as in in Fig. 2.

CH_3OH , and H_2CO without X-rays are much higher than those in the high-extinction ones. After we turn on the X-ray irradiation, the abundances become lower, but are still higher than those in the high-extinction regions. The high abundances in the gas are caused mainly by the high photo-evaporation rate on the grain surface. After we turn off X-rays, the gas abundances quickly

recover the values in the no-X-ray case, and hence the imprint of the X-rays disappears within about 10^6 years.

4.4. Age of Molecular Cloud

To see the response of a more evolved molecular cloud to the X-rays from the AGN, we run our chemical-reaction network without X-rays for 10^7 years and take the resulting chemical abundances as our new initial con-

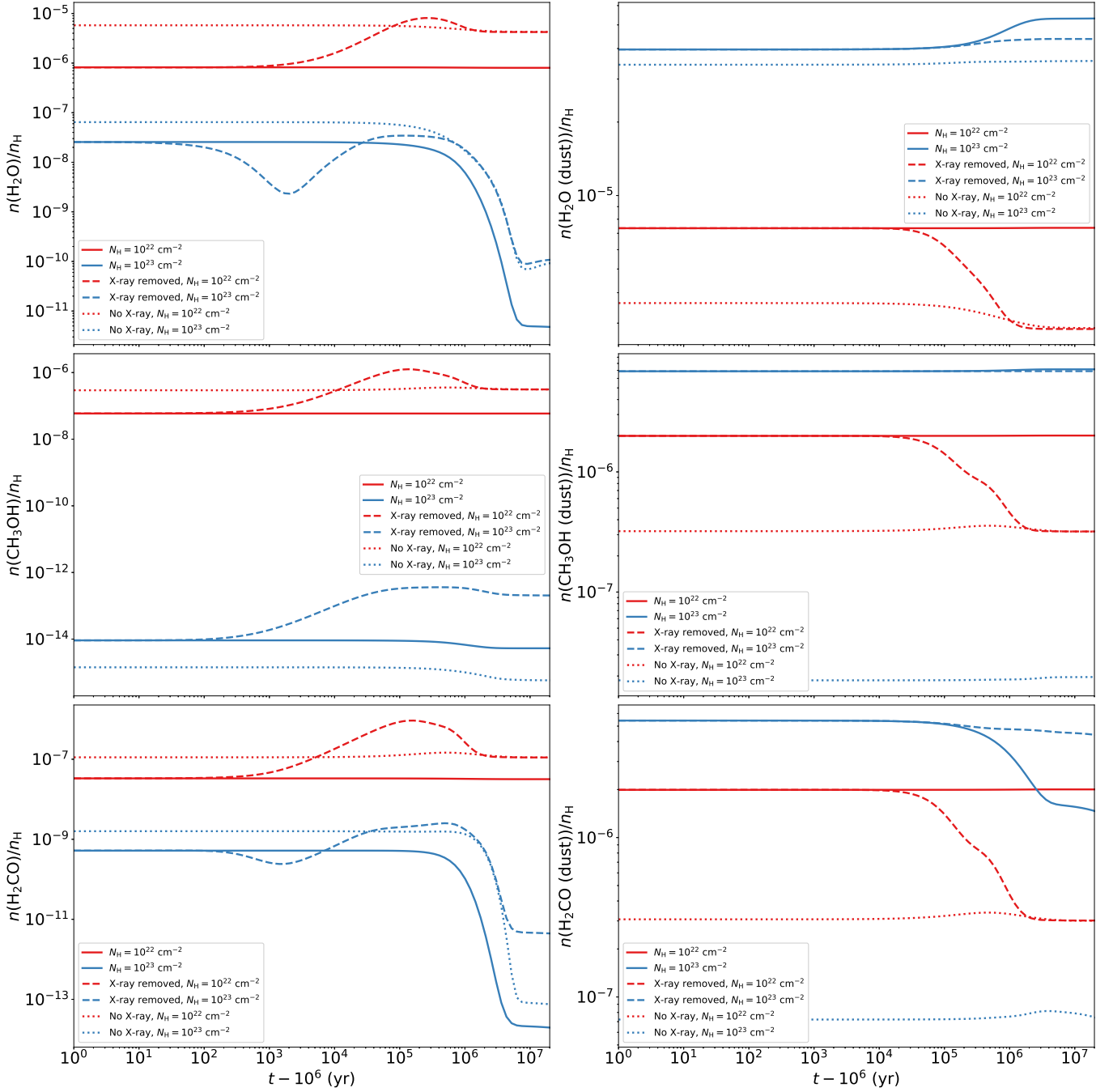


Figure 5. Abundances of H_2O , CH_3OH , and H_2CO (from top to bottom) at different depth of a molecular cloud, located at 4 kpc from the Galactic Center. The depth is proportional to the column density N_{H} . The red curves correspond to a column density of $N_{\text{H}} = 10^{22} \text{ cm}^{-2}$ and the blue ones to 10^{23} cm^{-2} . The left panels show the abundances in the gas phase and the right ones show the abundances on the grain surface.

dition for the later simulations. The other parameters are the same as in the fiducial model. The results are presented in Figure 6. We see that the abundances in the case without X-rays no longer significantly vary with time, both in the gas and on the grain surface, suggesting that the chemical reactions have reached an equilibrium on a timescale of 10^7 years.

If we turn on X-ray irradiation after the 10^7 years of isolated evolution, on the grain surface (right panels) the abundances of H_2O and CH_3OH will increase, as we have seen in the fiducial model, but the abundance of H_2CO decreases. The decrease is caused by the reaction $\text{H}_2\text{CO} + \text{H} \longrightarrow \text{HCO} + \text{H}_2$, which predominates in the current conditions. We notice that the variation of the abundances of CH_3OH and H_2CO after we turn on X-rays is not as prominent as that in a less evolved cloud (see our fiducial model). This difference indicates that a chemically more evolved cloud is more resilient to X-ray irradiation. After we remove the X-rays, the surface abundances return to the values in the case of no X-ray radiation, on a timescale of about 10^7 years.

In the gas phase (left panels), the X-ray irradiation significantly lowers the abundances of all the three molecules. This behavior is different from that in a less-evolved cloud, where the CH_3OH abundance is enhanced by X-rays (see Fig. 3). After we remove the X-rays, the abundances rise more quickly than that in a less-evolved cloud. As a result of the quick rise, a recovery of the equilibrium state for no X-rays is seen at about $10^4 - 10^5$ years. After this time, the imprint of an AGN is lost.

5. Diagnostics

Here we provide possible diagnostics for future observations by showing in Figure 7 the abundance ratios of H_2O , CH_3OH , and H_2CO with respect to CO. We choose CO as the reference because it is the second most abundant gas molecule (after H_2) and relatively easy to detect in molecular clouds. Molecules on the grain surface are not directly detectable, but we plot their abundance ratios relative to the gas-phase CO as well, because surface molecules could be rapidly released into the gas in certain processes which are not considered in this work, for example, by turbulence or shock (Federman & Allen 1991; García-Burillo et al. 2010; Harada et al. 2018). We show only the results from our fiducial model. The other models generally lead to the same conclusion.

The three blue panels labeled with “Gas” in Figure 7 show the abundance ratios in the gas phase. From these diagrams, we find that by the end of our simulations (marked by the star symbols), the locations of

the molecular clouds exposed to X-ray irradiation (solid and dashed curves) are well separated from those clouds without X-ray irradiation (dot-dashed curves). The divergence of the curves starts the earliest in the diagram of $\text{H}_2\text{CO}/\text{CO}$ against $\text{CH}_3\text{OH}/\text{CO}$. It is worth noting that at the column densities of our interest, the low-J transitions of H_2CO and CH_3OH are optically thin, therefore they are good tracers of the past activities of Sgr A*.

The three red panels labeled with “Dust” show the abundances of the H_2O , CH_3OH , and H_2CO on the grain surface relative to the gaseous abundance of CO. The evolutionary tracks with and without X-rays, as well as the final locations of the molecular clouds, are well separated in these diagrams. This result indicates that the molecular clouds showing strong signs of turbulence or shock could provide better diagnostics of the activity of Sgr A*, because the surface molecules could have been released into the gas.

For the other neutral species simulated in this work, their diagnostics are shown in Appendix B.

6. Caveats

Besides photo-desorption (see §2.3), X-rays could also excite an electron to a sufficiently high energy so that it escapes from the grain surface (Draine 2011). These photoelectrons from dust grains, in principle, are energetic enough to ionize the gas molecules, but we did not consider them in this work because of the uncertainty in the calculation of their number (Bakes & Tielens 1994; Weingartner & Draine 2001; Weingartner et al. 2006). The following estimation shows that by neglecting these photoelectrons, we could have underestimated the ionization rate of molecular gas by a factor of 2 – 9, and hence underestimated the effect of the AGN on the molecules in the gas phase.

Following the work of Weingartner et al. (2006) who modeled photoelectric emission from the grains exposed to extreme ultraviolet and X-ray radiation, we assume that (i) the typical dust particles are carbonaceous grains with a radius of $0.1\mu\text{m}$ (cross section $\sim 3 \times 10^{-10} \text{ cm}^2$), (ii) after each absorption of a hard-X-ray photon ($h\nu > 1 \text{ keV}$) the probability of a photoelectron (either primary or secondary) escaping the bulk solid is 0.1 – 1, and (iii) the photoionization cross section of hydrogen atom in ground state is 10^{-23} cm^2 at 1 keV. Moreover, we adopt the previous assumptions of a gas-to-dust ratio of 100 (in mass) and a typical grain density of 3 g/cm^3 . We find that the ratio between the number density of hydrogen atoms and that of carbonaceous grains is 8×10^{11} . Given these numbers, we find that for each X-ray photon of 1 keV the average yield of photoelec-

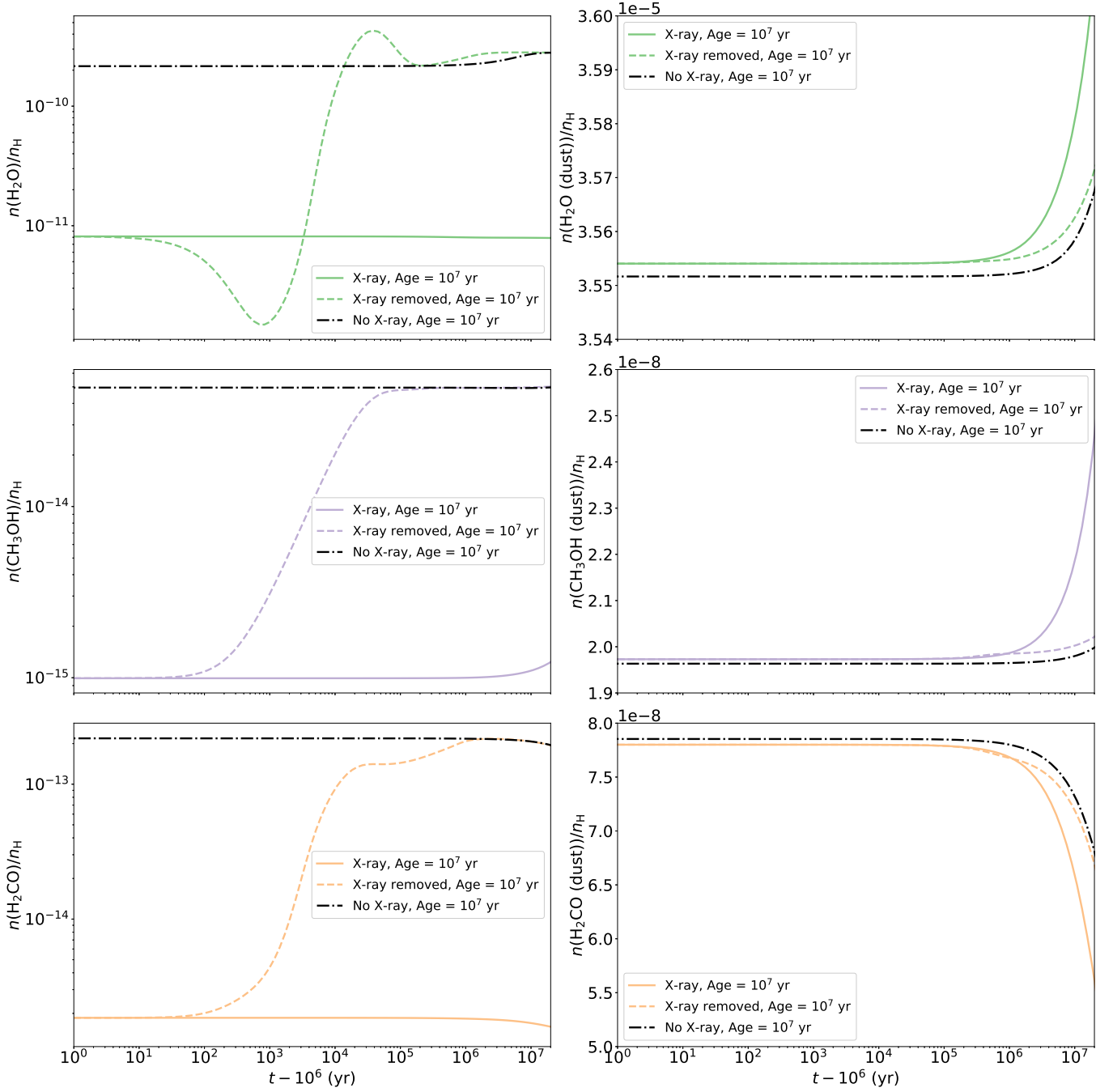


Figure 6. The same as in our fiducial model but the molecular clouds are 10^7 years old in the initial condition of our simulation.

trons from dust grains is about $24 - 240$. The exact number depends on the sizes of grains which is not well constrained by observations. However, it is about $0.8 - 8$ times the yield of photoelectrons from gaseous hydrogen (see §2.1). Therefore, the effect of the photoelectrons from dust grains deserves further investigation.

The loss of photoelectrons would leave the dust grains positively charged. The X-ray induced grain charging has not been modelled in detail until recently (e.g.

Ibáñez-Mejía et al. 2019). Charged grains, just like ambient electrons, can affect the temperature of free electrons through Coulomb scattering. They may also react with gaseous anions. However, both free electrons and gaseous anions are rare in the system of our interest. Therefore, we do not consider grain charging in this work.

7. Summary and Conclusion

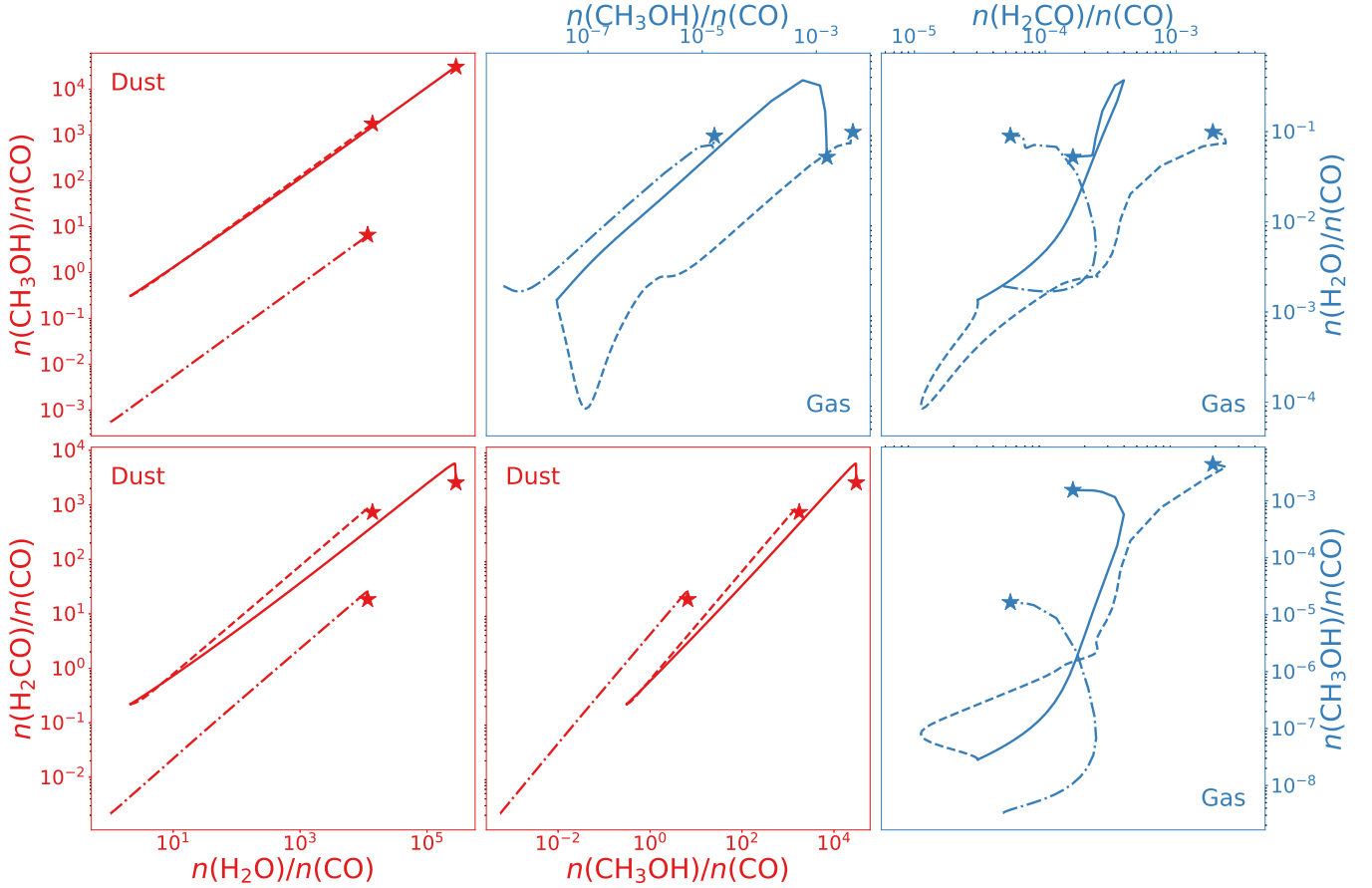


Figure 7. Diagnostics of the effect of X-ray irradiation on the molecular abundances. The abundances are calculated relative to the gas CO for easier comparison with observations. The three blue panels labeled with “Gas” refer to the abundances in the gas phase, and the red ones with “Dust” refer to the surface abundances. The curves correspond to the results from our fiducial model shown in Figs. 2 and 3. The line styles have the same meanings, i.e., the dot-dashed curves correspond to the evolution without X-rays, the solid ones correspond to the evolution with constant X-ray irradiation, and the dashed ones show the evolution when the X-ray is turned off after an initial 10^6 years of irradiation. The stars mark the end of our simulations, at the time of 5×10^7 years.

Motivated by the observational evidence that the SMBH in the Galactic Center could be an AGN several million years ago, we studied the impact of the corresponding X-ray irradiation on the molecular chemistry in the MW. Our main results are summarized as follows.

1. In our fiducial model, a molecular cloud is located at 4 kpc from the Galactic Center and has a column density of $10^{22.5} \text{ cm}^{-2}$. The X-ray irradiation from the AGN could slightly enhance the abundance of H_2O on the surface of dust grains and, at the same time, suppress the water abundance in the gas phase. After the AGN turns off, in the following 10^7 years, the abundance on the grain surfaces remains slightly higher than that in the case without X-rays, while the abundance in the gas phase almost recovers the value of the no-X-ray case.

2. For CH_3OH and H_2CO , our fiducial model shows that the abundances on the grain surface could be enhanced by one to two orders of magnitude during the X-ray irradiation. The enhancement could sustain for about 10^7 years even after the AGN is turned off. In the gas phase, the abundance of CH_3OH is enhanced during the AGN episode by about one order of magnitude, but that of H_2CO is reduced slightly. Interestingly, after we turn off the X-ray irradiation, both abundances rise significantly. Therefore, by the end of the 10^7 years of simulation, the final gas abundances are higher than the values in the no-X-ray case, by about two orders of magnitude.
3. The exact values of the molecular abundances during and after the AGN episode depend on the distance of the molecular cloud from the Galac-

tic Center. However, there is one feature which appears to be common at different Galactic distances. For a cloud similar to that in our fiducial model, if we irradiate it with X-ray for 10^6 years and then turn off the irradiation for 10^7 years, the final gas and the surface abundances are higher than the case with no X-ray irradiation. The enhancement is the most prominent at small Galactic distances, such as $\lesssim 2$ kpc.

4. After the AGN turns off, the recovery of the molecular abundances is faster in low-extinction regions ($N_H \lesssim 10^{22} \text{ cm}^{-2}$), such as the surface of a molecular cloud or a low-column-density cloud. Therefore, the imprint of a past AGN should be easier to observe in high-column-density regions, e.g., $N_H \gtrsim 10^{22.5} \text{ cm}^{-2}$.
5. Older molecular clouds (e.g. 10^7 years) recover more rapidly after the AGN turns off. Therefore, young molecular clouds are more likely to bear the chemical imprint of a past AGN.

These results suggest that the abundances of molecular species in the MW could be significantly affected and reach a new equilibrium during the past AGN activities of Sgr A*. The chemical imprint of the most recent AGN, which could have occurred several million years ago, may still be found today in those young, high-density molecular clouds residing at relatively small distances from the Galactic Center.

Acknowledgments

This project is under the framework of the Undergraduate Research and Training Program of Peking University and is sponsored by the National Innovation Training Program and School of Physics, Peking University. We thank Jieying Liu for kindly providing us with the AGN spectra of her numerical simulations and Zhu Liu for his help with the UV/X-ray extinction. We also thank Ke Wang, Guangshuai Zhang, Emma Yu, and Sarah Dodson-Robinson for compiling a reading list of the relevant literatures. X.C. acknowledges the supported by the NSFC grant Nos. 11721303 and 11991053. F.D. is supported by the Hundred-Talent Program (Chinese Academy of Sciences) through grant 2017-089 and by grants from NSFC (No. 11873094 and 11873097).

Appendix A Surface Reaction Network

Table 1 shows surface reactions in our model selected from the network in Hasegawa et al. (1992). The last column shows the reaction barrier.

Table 1. Surface reaction network.

Reactant 1	Reactant 2	Product 1	Product 2	E_a (K)
H	H	H ₂		0
H	C	CH		0
H	N	NH		0
H	O	OH		0
H	CH	CH ₂		0
H	NH	NH ₂		0
H	OH	H ₂ O		0
H	C ₂	C ₂ H		0
H	CN	HCN		0
H	CO	HOC		1000
H	CO	HCO		1000
H	NO	HNO		0
H	O ₂	O ₂ H		1200
H	N ₂	N ₂ H		1200
H	CH ₂	CH ₃		0
H	NH ₂	NH ₃		0
H	C ₂ H	C ₂ H ₂		0
H	HOC	CHOH		0
H	HCO	H ₂ CO		0
H	O ₂ H	H ₂ O ₂		0
H	O ₃	O ₂	OH	450
H	C ₂ N	HCCN		0
H	N ₂ H	N ₂ H ₂		0
H	CH ₃	CH ₄		0
H	H ₂ CO	HCO	H ₂	1850
H	CHOH	CH ₂ OH		0
H	H ₂ O ₂	H ₂ O	OH	1400
H	N ₂ H ₂	N ₂ H	H ₂	650
H	HCCN	CH ₂ CN		0
H	C ₂ H ₂	C ₂ H ₃		1210
H	C ₂ H ₃	C ₂ H ₄		0
H	CH ₂ OH	CH ₃ OH		0
H	CH ₂ CN	CH ₃ CN		0
H	C ₂ H ₄	C ₂ H ₅		750
H	C ₂ H ₅	C ₂ H ₆		0
H ₂	OH	H ₂ O	H	2600

Table 1 *continued*

Table 1 (*continued*)

Reactant 1	Reactant 2	Product 1	Product 2	E_a (K)
C	C	C ₂		0
C	N	CN		0
C	O	CO		0
C	CH	C ₂ H		0
C	NH	HNC		0
C	OH	HOC		0
C	OH	CO	H	0
C	CN	C ₂ N		0
C	NO	OCN		0
C	O ₂	CO	O	0
C	CH ₂	C ₂ H ₂		0
C	NH ₂	HNC	H	0
C	OCN	CO	CN	0
C	CH ₃	C ₂ H ₃		0
N	N	N ₂		0
N	O	NO		0
N	CH	HCN		0
N	NH	N ₂ H		0
N	C ₂	C ₂ N		0
N	NH ₂	N ₂ H ₂		0
O	O	O ₂		0
O	CH	HCO		0
O	NH	HNO		0
O	OH	O ₂ H		0
O	CN	OCN		0
O	O ₂	O ₃		0
O	CO	CO ₂		0
O	HCO	CO ₂	H	0
O	CH ₂	H ₂ CO		0
O	CH ₃	CH ₂ OH		0
CH	CH	C ₂ H ₂		0
CH	OH	CHOH		0

CH	HNO	NO	CH ₂	0
CH	CH ₃	C ₂ H ₄		0
OH	OH	H ₂ O ₂		0
OH	CH ₂	CH ₂ OH		0

Appendix B Other Important Molecular Species

We also calculated the evolution of several other species that are often observed in molecular clouds, including two molecular ions (HCO^+ , N_2H^+) and six neutral species (NH_3 , CH_4 , CO , HCN , OH , CH_3CN). The abundances on the grain surface and in the gas phase are shown, respectively, in Figures B1 and B2. The Calculation is conducted assuming our fiducial condition.

On the grain surface, the abundances of NH_3 , CH_4 , HCN , OH are enhanced by X-rays, while those of CO and CH_3CN slightly decrease in the presence of X-ray irradiation. In the gas phase, most of these molecular species tend to show lower concentration under X-ray irradiation. When we turn off the AGN, for most species the gas abundances quickly recover, but CH_4 shows a significant excess compared to the abundance in the case without X-rays. HCO^+ and N_2H^+ are temporarily produced in higher efficiency in the first 10^6 years of X-ray irradiation, and then the abundances decrease to values lower than those in the case without X-rays.

For completeness, we also plot in Figure B3 the diagnostics using all the neutral species shown above. We find that in the gas phase (blue panels), the evolutionary tracks with and without X-ray irradiation are well separated. Therefore, we conclude that the gas abundances of the neutral molecules studied in this work could be good tracers of the past AGN in the Galactic Center. The evolutionary tracks of the dust species (red panels) are also separated, except for the pairs $\text{H}_2\text{CO}-\text{CH}_4$, $\text{H}_2\text{O}-\text{HCN}$, $\text{H}_2\text{O}-\text{CH}_3\text{CN}$, and $\text{HCN}-\text{CH}_3\text{CN}$.

References

- Ádámkóvics, M., Glassgold, A. E., & Meijerink, R. 2011, *ApJ*, 736, 143
- Allen, M., & Robinson, G. W. 1977, *ApJ*, 212, 396
- Amaro-Seoane, P., & Chen, X. 2019, *JCAP*, 2019, 056
- Bakes, E. L. O., & Tielens, A. G. G. M. 1994, *ApJ*, 427, 822
- Balbi, A., & Tombesi, F. 2017, *Scientific Reports*, 7, 16626
- Bergin, E. A., & Tafalla, M. 2007, *ARA&A*, 45, 339
- Bland-Hawthorn, J., Maloney, P. R., Sutherland, R. S., & Madsen, G. J. 2013, *ApJ*, 778, 58
- Carey, S. J., Clark, F. O., Egan, M. P., et al. 1998, *ApJ*, 508, 721
- Chang, Q., & Herbst, E. 2014, *ApJ*, 787, 135
- Chen, H., Forbes, J. C., & Loeb, A. 2018, *ApJL*, 855, L1
- Chen, X., & Amaro-Seoane, P. 2015, *Classical and Quantum Gravity*, 32, 064001
- Clarke, J. N. 1981, *Icarus*, 46, 94
- Davies, R., Mark, D., & Sternberg, A. 2012, *A&A*, 537, A133
- Draine, B. T. 1978, *ApJS*, 36, 595
- . 2011, *Physics of the Interstellar and Intergalactic Medium*, Princeton: Princeton University Press
- Federman, S. R., & Allen, M. 1991, *ApJ*, 375, 157

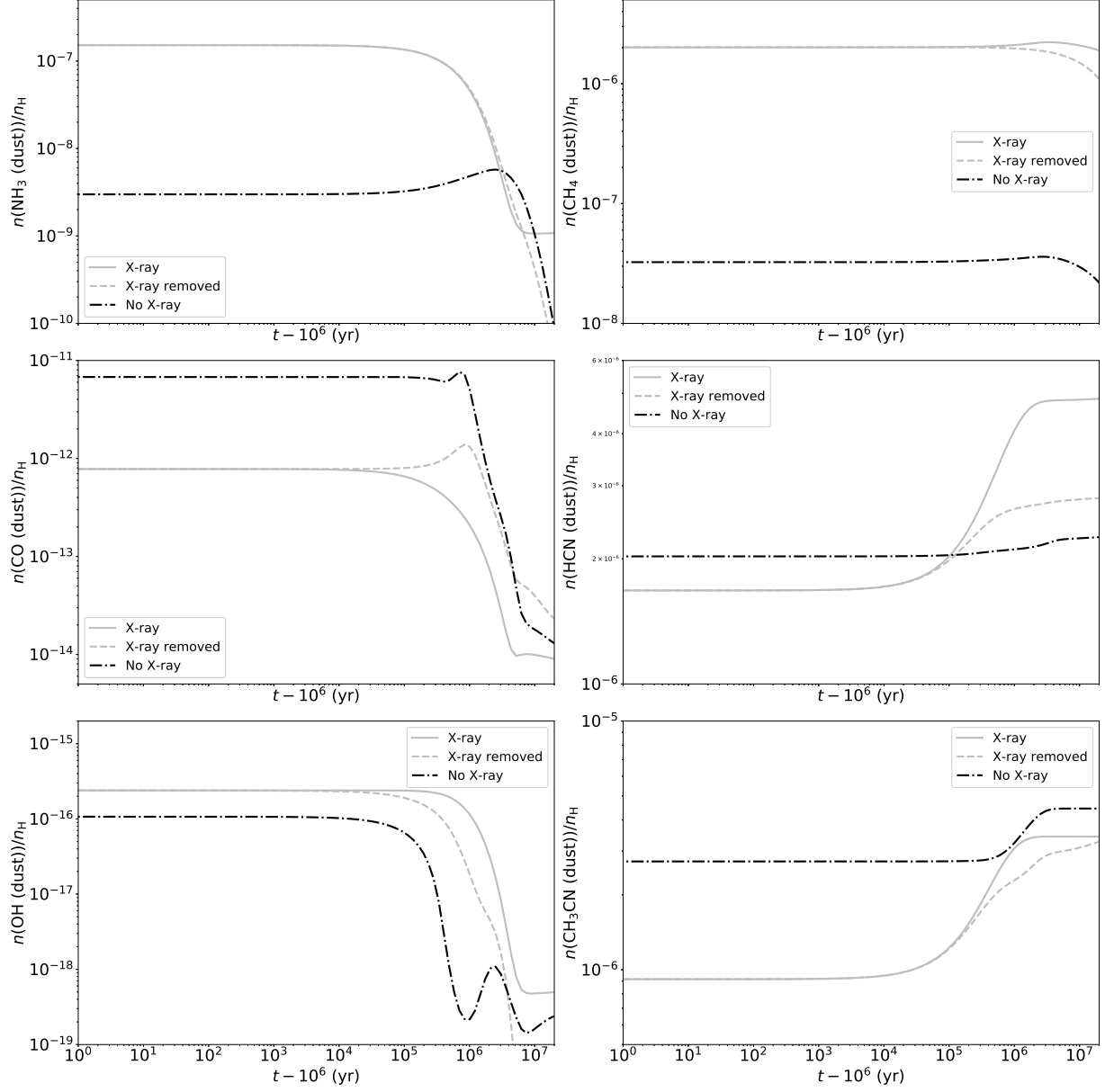


Figure B1. Abundances of NH_3 , CH_4 , CO , HCN , OH , CH_3CN on the grain surface as a function of time in our fiducial model.

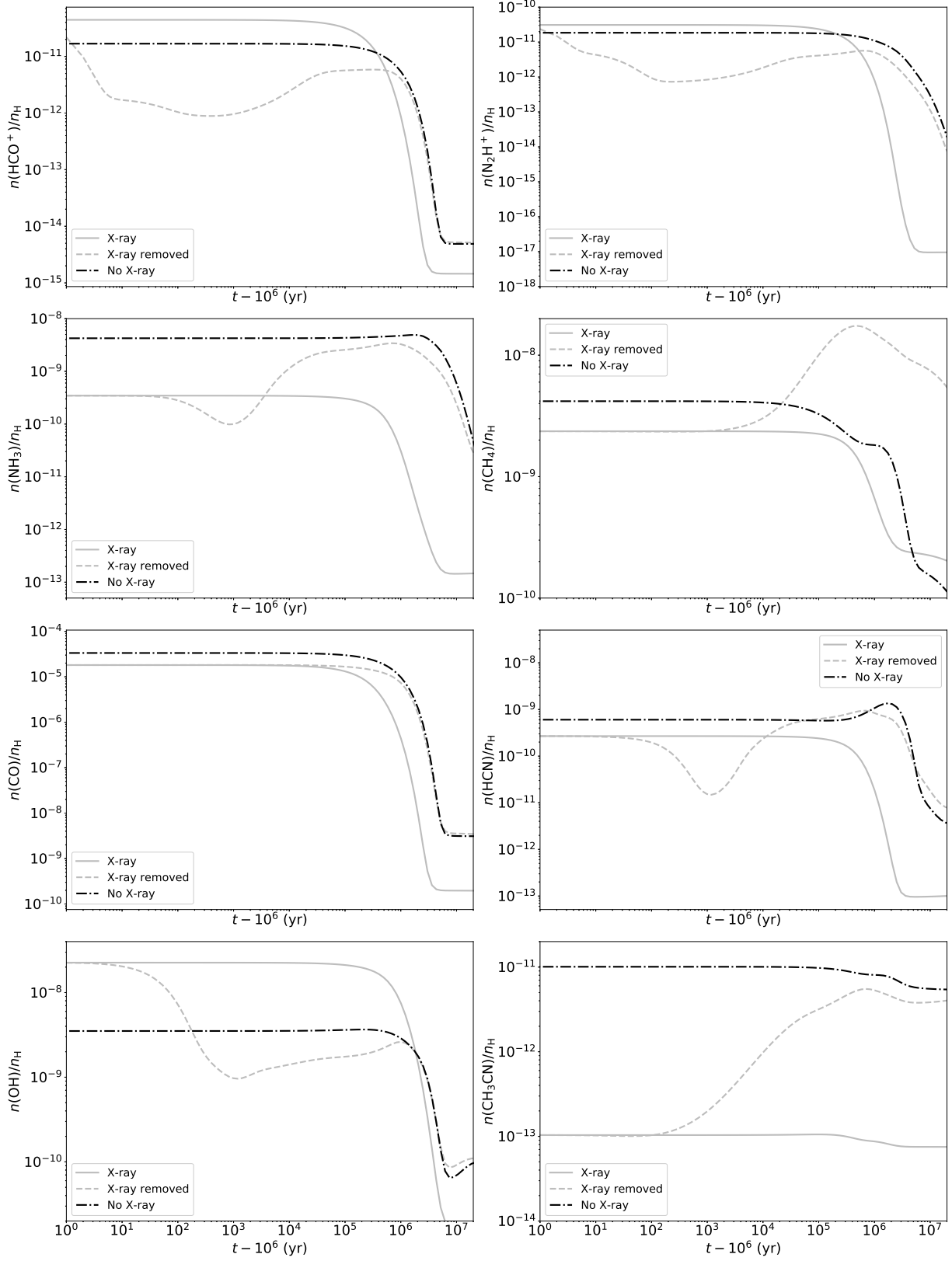


Figure B2. Same as Fig. B1 but for the molecules in the gas phase. Two molecular ions (HCO^+ and N_2H^+) are also included

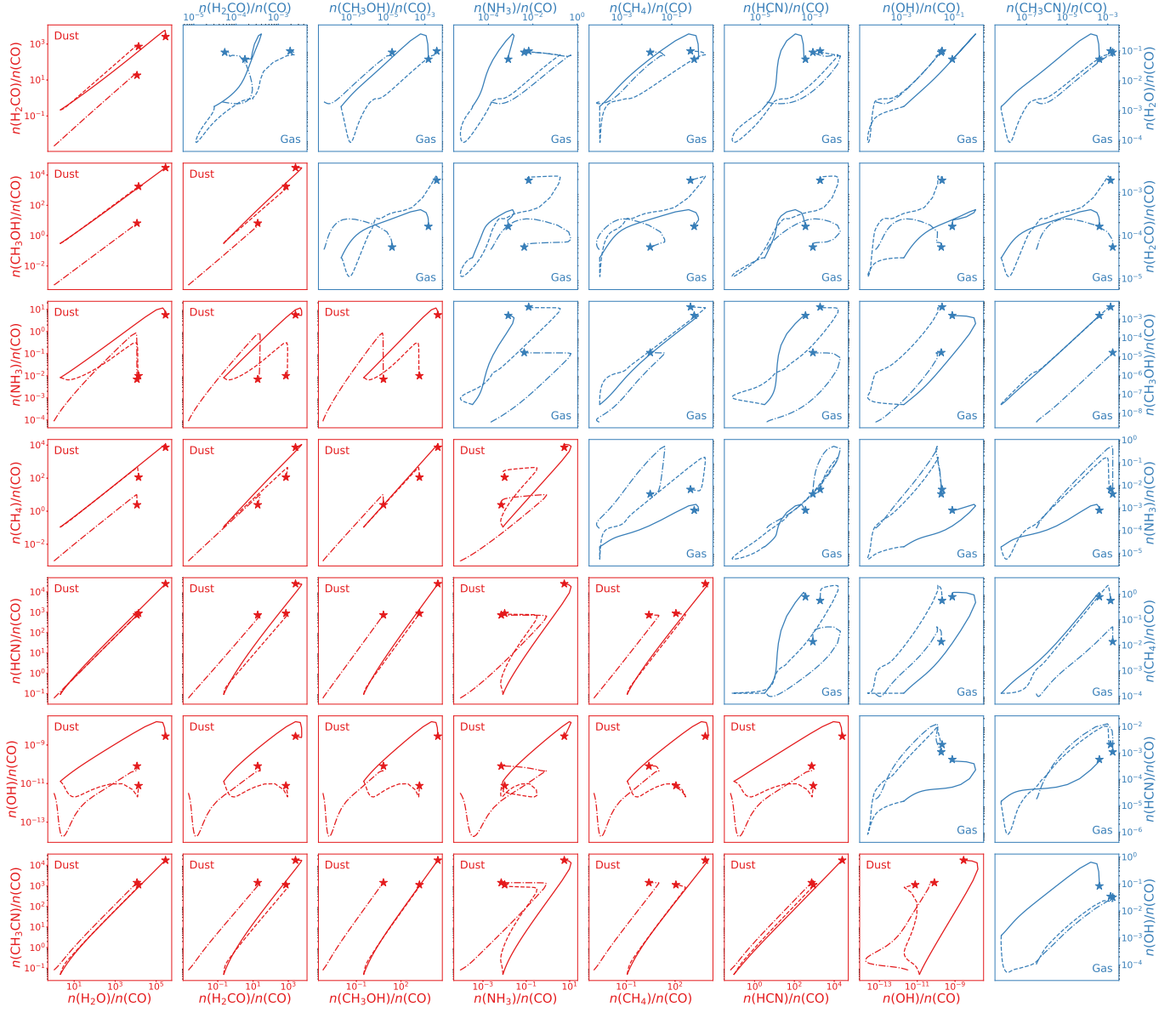


Figure B3. Same as Fig. 7, but shows all the neutral species listed in Appendix B.

- Forbes, J. C., & Loeb, A. 2018, *MNRAS*, 479, 171
- García-Burillo, S., Combes, F., Usero, A., et al. 2014, *A&A*, 567, A125
- García-Burillo, S., Usero, A., Fuente, A., et al. 2010, *A&A*, 519, A2
- Garrod, R. T., & Pauly, T. 2011, *ApJ*, 735, 15
- Garrod, R. T., Widicus Weaver, S. L., & Herbst, E. 2008, *ApJ*, 682, 283
- Genzel, R., Eisenhauer, F., & Gillessen, S. 2010, *Reviews of Modern Physics*, 82, 3121
- Goldsmith, P. F. 2001, *ApJ*, 557, 736
- Gonzalez, G. 2005, *Origins of Life and Evolution of the Biosphere*, 35, 555
- González-Alfonso, E., Fischer, J., Isaak, K., et al. 2010, *A&A*, 518, L43
- Grassi, T., Bovino, S., Schleicher, D. R. G., et al. 2014, *MNRAS*, 439, 2386
- Harada, N., Sakamoto, K., Martín, S., et al. 2018, *ApJ*, 855, 49
- Harada, N., Riquelme, D., Viti, S., et al. 2015, *A&A*, 584, A102
- Hasegawa, T. I., & Herbst, E. 1993, *MNRAS*, 261, 83
- Hasegawa, T. I., Herbst, E., & Leung, C. M. 1992, *ApJS*, 82, 167
- Herbst, E., & Klemperer, W. 1973, *ApJ*, 185, 505
- Herbst, E., & van Dishoeck, E. F. 2009a, *ARA&A*, 47, 427
- . 2009b, *ARA&A*, 47, 427
- Hopkins, P. F., & Hernquist, L. 2009, *ApJ*, 698, 1550
- Hopkins, P. F., Hernquist, L., Cox, T. J., et al. 2006, *ApJS*, 163, 1
- Ibáñez-Mejía, J. C., Walch, S., Ivlev, A. V., et al. 2019, *MNRAS*, 485, 1220
- Imanishi, M., & Nakanishi, K. 2014, *AJ*, 148, 9
- Izumi, T., Kohno, K., Aalto, S., et al. 2015, *ApJ*, 811, 39
- Jiménez-Escobar, A., Ciaravella, A., Cecchi-Pestellini, C., et al. 2018, *ApJ*, 868, 73
- Kohno, K., Ishizuki, S., Matsushita, S., Vila-Vilaró, B., & Kawabe, R. 2003, *PASJ*, 55, L1
- Kormendy, J., & Ho, L. C. 2013, *ARA&A*, 51, 511
- Krolik, J. H., & Kallman, T. R. 1983, *ApJ*, 267, 610
- Latif, M. A., Bovino, S., Grassi, T., Schleicher, D. R. G., & Spaans, M. 2015, *MNRAS*, 446, 3163
- Laviolette, P. A. 1987, *Earth Moon and Planets*, 37, 241
- Lepp, S., & Dalgarno, A. 1996, *A&A*, 306, L21
- Lingam, M., Ginsburg, I., & Bialy, S. 2019, *ApJ*, 877, 62
- Liu, J. Y., Qiao, E. L., & Liu, B. F. 2016, *ApJ*, 833, 35
- Maloney, P. R., Hollenbach, D. J., & Tielens, A. G. G. M. 1996, *ApJ*, 466, 561
- Martín, S., Kohno, K., Izumi, T., et al. 2015, *A&A*, 573, A116
- McMillan, P. J. 2017, *MNRAS*, 465, 76
- Meijerink, R., & Spaans, M. 2005, *A&A*, 436, 397
- Meijerink, R., Spaans, M., & Israel, F. P. 2007, *A&A*, 461, 793
- Mezger, P. G., Duschl, W. J., & Zylka, R. 1996, *A&A Rv*, 7, 289
- Nakajima, T., Takano, S., Kohno, K., et al. 2015, *PASJ*, 67, 8
- Nayakshin, S., & Cuadra, J. 2005, *A&A*, 437, 437
- Quan, D., & Herbst, E. 2007, *A&A*, 474, 521
- Shankar, F., Weinberg, D. H., & Miralda-Escudé, J. 2009, *ApJ*, 690, 20
- Shull, J. M., & van Steenberg, M. E. 1985, *ApJ*, 298, 268
- Snell, R. L., Howe, J. E., Ashby, M. L. N., et al. 2000, *ApJL*, 539, L101
- Soltan, A. 1982, *MNRAS*, 200, 115
- Stäuber, P., Doty, S. D., van Dishoeck, E. F., & Benz, A. O. 2005, *A&A*, 440, 949
- Su, M., Slatyer, T. R., & Finkbeiner, D. P. 2010, *ApJ*, 724, 1044
- Takano, S., Nakajima, T., Kohno, K., et al. 2014, *PASJ*, 66, 75
- Tielens, A. G. G. M. 2010, *The Physics and Chemistry of the Interstellar Medium*, Cambridge, UK: Cambridge University Press
- Usero, A., García-Burillo, S., Fuente, A., Martín-Pintado, J., & Rodríguez-Fernández, N. J. 2004, *A&A*, 419, 897
- Verner, D. A., Ferland, G. J., Korista, K. T., & Yakovlev, D. G. 1996, *ApJ*, 465, 487
- Visser, R., Doty, S. D., & van Dishoeck, E. F. 2011, *A&A*, 534, A132
- Viti, S., García-Burillo, S., Fuente, A., et al. 2014, *A&A*, 570, A28
- Volonteri, M. 2010, *A&A Rv*, 18, 279
- Wakelam, V., & Herbst, E. 2008, *ApJ*, 680, 371
- Wakelam, V., Smith, I. W. M., Herbst, E., et al. 2010, *SSRv*, 156, 13
- Weingartner, J. C., & Draine, B. T. 2001, *ApJS*, 134, 263
- Weingartner, J. C., Draine, B. T., & Barr, D. K. 2006, *ApJ*, 645, 1188
- Wisłocka, A. M., Kovačević, A. B., & Balbi, A. 2019, *A&A*, 624, A71